Surface elastic waves in solid composites of two-dimensional periodicity

B. Manzanares-Martínez
Programa de Posgrado en Ciencias (Física) de la Universidad de Sonora, Calle Rosales y Boulevard Luis Encinas, Hermosillo, Sonora 83000, México

F. Ramos-Mendieta
Centro de Investigación en Física de la Universidad de Sonora, Apartado Postal 5-088, Hermosillo, Sonora 83190, México
(Received 10 November 2002; revised manuscript received 6 August 2003; published 3 October 2003)

We have studied the elastic surface waves in a truncated two-dimensional solid composite. The periodic structure is constituted by a square array of parallel tungsten (W) cylinders embedded in silicon (Si). The surface plane that terminates the crystal cuts perpendicularly the plane of periodicity along the (10) direction. Thus the surface plane is parallel to the axes of a row of cylinders. We found that surface waves can propagate with wave vector laying along the one dimensional surface periodicity that results from the truncation. Both mixed and transverse polarizations were considered, but only surface waves of mixed polarization exist when the truncation leaves complete cells at the surface. We have also studied the guidance of elastic waves by a homogeneous layer of Si grown at the surface of the crystal. The wave confinement within this adlayer is possible due to the scattering effects suffered by the field of displacement inside the periodic structure at frequencies in the band gaps.

DOI: 10.1103/PhysRevB.68.134303 PACS number(s): 43.20.+g, 43.40.+s, 62.30.+d, 68.35.Ja

I. INTRODUCTION

It is known that elastic vibrations in the periodic arrays called phononic crystals (PCs) satisfy a frequency band structure.[1–6] This means that depending on their structural and material parameters the PCs can support frequency ranges of forbidden wave propagation—*the band gaps*. This ability to avoid the propagation of acoustic energy in specific frequency ranges gives these artificial material potential applications in transducer and filter technology.[7–10]

Up to now the properties of the acoustic bulk bands in two-dimensional (2D) crystals have been a well studied topic. Several reports of arrays of solid cylinders embedded in fluids or in a different solid, with materials as aluminum (Al), copper (Cu), polymers, mercury (Hg), air, etc., have shown the existence of band gaps.[11–16] In addition, surface waves in truncated crystals have been also studied in structures with the plane of truncation parallel to the plane of periodicity.[17–19] The waves propagate along the 2D periodic surface and decay exponentially into the crystal. Although scattering effects are present on the plane of propagation, we may say that these waves are of Rayleigh type because their amplitude decays along the direction of homogeneity—the direction perpendicular to the plane of periodicity.

There exists, however, another configuration that also supports elastic surface waves. In this paper we shall present some properties of the surface waves in a 2D PC of square symmetry with the plane of truncation parallel to the axes of a row of cylinders. The surface (now of implicit one-dimensional periodicity) cuts the crystal through the interstitial region (see Fig. 1). In addition to the Rayleigh-type waves for which the displacement amplitude decays exponentially into the crystal, a special type of vibration confinement at the surface occurs due to the coherent scattering of the waves inside the crystal. As we shall see, in the latter case the elastic displacement oscillates in the direction perpendicular to the surface, but decays with an exponential modulation.

Experimental evidence in a solid/fluid system that shows the existence of surface waves was recently published.[1] An square array of Hg cylinders in Al with a lattice constant $a = 2.8$ mm exhibited a surface vibration at the frequency of 0.75 MHz. However, in spite of the accessibility of these results, we are not aware of a report treating these waves in solid/solid composites. In what follows we present a numerical study of these waves in a crystal of W cylinders in Si (impedance average contrast $Z_W/Z_{Si}=4.2$). The results are representative of the general behavior (similar surface waves were also found in systems of W cylinders in Al and Cu cylinders in Al). The only requirement is a relative high impedance contrast in order to produce band gaps as large as possible for hosting the dispersion relation $\omega(k)$ of the surface waves. All the calculations were made employing ma-

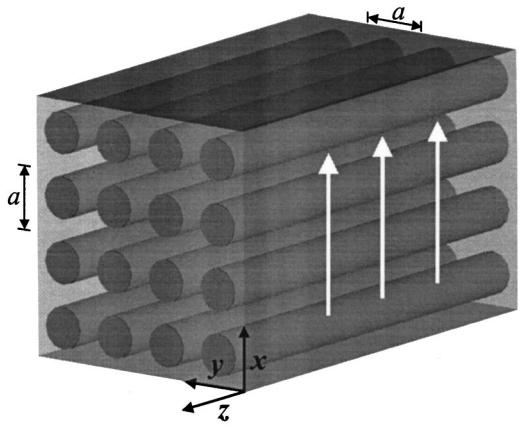

FIG. 1. The truncated crystal with *x,z* the cutting plane. The surface is defined by $y=0$. The arrows represent the direction of propagation of surface waves.

terial parameters corresponding to the isotropic approximation.

The paper is organized as follows. In Sec. II we present the basic equations that govern the problem. Particular emphasis is placed in the supercell method that is useful to obtain localized modes and surface waves. In Sec. III we show numerical results and discuss the physical properties of the surface vibrations. Finally, in Sec. IV the conclusions are given.

II. THEORY

The crystal is composed of parallel solid cylinders of mass density ρ_a, transverse velocity c_{ta}, and longitudinal velocity c_{la} embedded in a different solid of parameters ρ_b, c_{tb}, and c_{lb}. The array is square on the x,y plane; $f=\pi R^2/a^2$ is the filling fraction, with R and a the radius of the cylinders and the lattice constant, respectively. Mathematically the crystal is defined by the periodic mass density $\rho(\vec{r})=\rho(\vec{r}+\vec{c})$ and velocities $c_t(\vec{r})=c_t(\vec{r}+\vec{c})$, and $c_l(\vec{r})=c_l(\vec{r}+\vec{c})$, where $\vec{r}=x\hat{i}+y\hat{j}$ and $\vec{c}=c_x\hat{i}+c_y\hat{j}$ are the 2D position vector and crystal translation vector, respectively. The bulk modes in the structure are governed by the equations

$$\rho\frac{\partial^2 u_\mu}{\partial t^2}=\frac{\partial\sigma_{\mu x}}{\partial x}+\frac{\partial\sigma_{\mu y}}{\partial y},\quad \mu=x,y,z \tag{1}$$

where $\vec{u}(x,y,t)=(u_x,u_y,u_z)$ is the vector of displacement. The stress tensor has the components

$$\sigma_{\mu\nu}=\rho c_t^2\left(\frac{\partial u_\mu}{\partial\nu}+\frac{\partial u_\nu}{\partial\mu}\right)+\rho(c_l^2-2c_t^2)(\nabla\cdot\vec{u})\delta_{\mu\nu}, \tag{2}$$

with $\mu,\ \nu\rightarrow x,\ y,\ z$. Due to the crystalline periodicity the solutions must satisfy the Bloch theorem. Then,

$$\vec{u}(x,y,t)=\exp(i\vec{k}\cdot\vec{x})\sum_{\vec{G}}\vec{u}_{\vec{G}}(\vec{k})\exp(i\vec{G}\cdot\vec{x})\exp(-i\omega t), \tag{3}$$

where $\vec{k}=k_x\hat{i}+k_y\hat{j}$ is the Bloch wave vector and $\hat{G}=(2\pi/a)(n\hat{i}+m\hat{j})$, with n and m integers, are the reciprocal lattice vectors (we are expanding the periodic part of the solution with an infinite basis of plane waves). Taking into account the periodicity of both the mass density and the elastic constants, we expand each function ρ, ρc_l^2, and ρc_t^2 in a Fourier series employing the same $\vec{G}$ basis. By substituting Eqs. (2) and (3) into Eq. (1) we obtain the next matrix relation:

$$\begin{pmatrix} M_{xx}^{\vec{G}\vec{G}'} & M_{xy}^{\vec{G}\vec{G}'} & 0 \\ M_{yx}^{\vec{G}\vec{G}'} & M_{yy}^{\vec{G}\vec{G}'} & 0 \\ 0 & 0 & M_{zz}^{\vec{G}\vec{G}'} \end{pmatrix}\begin{pmatrix} u_x(\vec{G}') \\ u_y(\vec{G}') \\ u_z(\vec{G}') \end{pmatrix} = \omega^2 N_{\vec{G}\vec{G}'}\begin{pmatrix} 1 & 0 & 0 \\ 0 & 1 & 0 \\ 0 & 0 & 1 \end{pmatrix}\begin{pmatrix} u_x(\vec{G}') \\ u_y(\vec{G}') \\ u_z(\vec{G}') \end{pmatrix}. \tag{4}$$

The matrix elements are

$$M_{xx}^{\vec{G}\vec{G}'}=(k_x+G_x')(k_x+G_x)\lambda(\vec{G}-\vec{G}')+(k_y+G_y)(k_y+G_y')\tau(\vec{G}-\vec{G}'),$$

$$M_{xy}^{\vec{G}\vec{G}'}=(k_x+G_x')(k_y+G_y)\tau(\vec{G}-\vec{G}')+[\lambda(\vec{G}-\vec{G}')-2\tau(\vec{G}-\vec{G}')](k_x+G_x)(k_y+G_y'),$$

$$M_{yx}^{\vec{G}\vec{G}'}=(k_x+G_x)(k_y+G_y')\tau(\vec{G}-\vec{G}')+[\lambda(\vec{G}-\vec{G}')-2\tau(\vec{G}-\vec{G}')](k_x+G_x')(k_y+G_y),$$

$$M_{yy}^{\vec{G}\vec{G}'}=(k_x+G_x)(k_x+G_x')\tau(\vec{G}-\vec{G}')+(k_y+G_y')(k_y+G_y)\lambda(\vec{G}-\vec{G}'),$$

$$N_{\vec{G}\vec{G}'}=\rho(\vec{G}-\vec{G}'),$$

where $\lambda(\vec{G})$, $\tau(\vec{G})$, and $\rho(\vec{G})$ are the coefficients of the Fourier expansions for $\rho c_l^2(\vec{x})$, $\rho c_t^2(\vec{x})$ and $\rho(\vec{x})$, respectively. [Each one of these three latter functions has a position dependence of the form $\chi(\vec{x})=\chi_b+(\chi_a-\chi_b)\Theta(R-|\vec{x}|)$, where χ_a and χ_b are the constant value of the corresponding parameter inside the rods or in the interstitial region, respectively, and $\Theta(\alpha)$ is the Heaviside function ($\Theta=1$ for $\alpha\geqslant 0$, $\Theta=0$ for $\alpha<0$).] The Fourier coefficients $X(\vec{G})$ are derived from the integral equation

$$X(\vec{G})=\frac{1}{A_c}\int_{A_c}\chi(\vec{x})\exp(-\vec{G}\cdot\vec{x})d^2x,$$

in which A_c is the unit cell area. The final expression has the form

$$X(\vec{G})=\chi_b\delta_{\vec{G},0}+2(\chi_a-\chi_b)J_1(GR)(1-\delta_{\vec{G},0})/GR,$$

where J_1 is a Bessel function of first kind.]

As can be easily deduced, Eq. (4) describes two types of independent bulk vibrations that propagate with wave vector on the plane of periodicity. One, the waves of mixed polarization with compressional and shear components ($\vec{u}=u_x\hat{i}+u_y\hat{j}$), and two, the transverse (shear) waves, with the displacement vector $\vec{u}=u_z\hat{k}$.

In calculating the elastic surface modes of truncated crystals Eq. (4) is also useful. The only requirement is the appropriate definition of a supercell. In reality, Eq. (4) allows one to obtain the surface modes in a crystal slab with surfaces resembling the surface of the truncated crystal. The thicker the slab, the smaller the interaction between the modes localized at each one of the two slab surfaces. Then, the dispersion relation of such modes is expected to converge to that of the surface modes in a semi-infinite structure.

As an example, in Fig. 2 we show the half part of a symmetric supercell associated with a crystal slab of seven layers, $L_s=7a$. Note that the repetition of this supercell at the sites $\vec{r}_{nm}=na\hat{i}+mL\hat{j}$, with n and m integers, produces

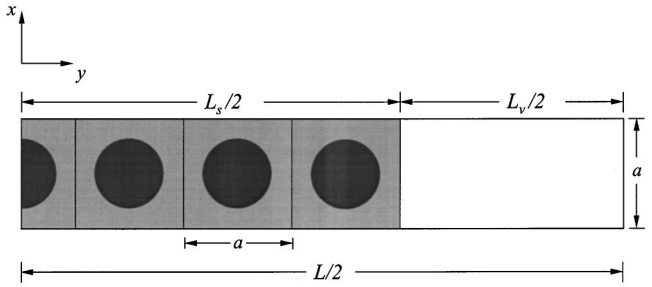

FIG. 2. One half of the supercell. In this example the supercell has $n=7$ complete cells. The supercell contains a slab of W cylinders embedded in Si bounded by vacuum on both sides.

an array of alternating crystal and vacuum slabs. The key to the supercell method when surface modes are studied is the calculation of the frequency bands in this array; some bands projected on the plane of the surface will correspond precisely to the surface vibrations. When both the vacuum region and the crystal slab are thick enough, the bands associated with the surface modes will be very narrow with frequencies lying inside the bulk gaps of the infinite crystal. The narrow bands that approach the curves of degenerate modes correspond to the dispersion relations of the surface waves in the semi-infinite crystal. For details of the supercell method, see Ref. 20.

In defining the supercell the most important issue is the selection of the medium that we are naming vacuum. As is known, the supercell method demands a finite interaction, small as possible, between the modes of neighboring crystal slabs. In order to allow the displacement field to penetrate the vacuum regions we need to replace the real vacuum by a convenient (artificial) material. The only condition is to choose the parameters properly in order to ensure the rapid decay of the displacement amplitude—the shorter the penetration into the ''vacuum'' the better the approximation to the real situation. From the boundary conditions at the interface of the crystal-vacuum we can estimate the values of the mass density and the sound velocities that will define the artificial medium. The normal and tangential stress components which are continuous through the interface are

$$\sigma_{yy}=\rho(c_l^2-c_t^2)\frac{\partial u_x}{\partial x}+\rho c_l^2\frac{\partial u_y}{\partial y}, \tag{5}$$

$$\sigma_{yx}=\rho c_t^2\left[\frac{\partial u_x}{\partial y}+\frac{\partial u_y}{\partial x}\right]. \tag{6}$$

Allowing finite variations of the amplitude near the interface, Eqs. (5) and (6) resemble the condition of a solid-vacuum interface only when the mass density and the sound velocities of the artificial medium satisfy $\rho c_{t,l}^2\to 0$ (A solid-vacuum interface is stress free. Thus $\sigma_{yy}=\sigma_{yx}=0$.) In order to avoid numerical conflicts, in practice the values of $\rho c_{t,l}^2$ for the auxiliary medium are chosen to be as low as possible with respect to their values for the constitutive materials of the crystal. Thus the previous absolute condition needs be replaced by

$$\frac{\rho c_{l,t}^2}{(\rho c_{l,t}^2)_{W,\mathrm{Si}}}\to 0. \tag{7}$$

It is natural to select a small mass density ρ. However, for the velocities there exists an additional condition. We know that the wave vector component in the perpendicular direction to the surface is $k_y=(\omega^2/c_{l,t}^2-k_x^2)^{1/2}$. This means that the exponential decay of vibrations occurs when $k_x>\omega/c_{l,t}$. Therefore, it is required for the auxiliary medium that the transverse and longitudinal velocities be finite quantities. In fact they must be high enough (three or four orders of magnitude higher than the velocities of the constitutive materials) to allow one the calculation of the surface modes of the small wave vector k_x. The numerical results of Sec. III were obtained with the artificial vacuum satisfying $\rho=10^{-7}$ gr/cm^3 and $\rho c_t^2=\rho c_l^2=10^{10}$ gr/(cm s^2). For the constitutive materials we have [in units of gr/(cm s^2)]: $\rho_W c_{tW}^2=1.5\times 10^{12}$, $\rho_W c_{lW}^2=5.0\times 10^{12}$, $\rho_{\mathrm{Si}} c_{t\mathrm{Si}}^2=0.8\times 10^{12}$, and $\rho_{\mathrm{Si}} c_{l\mathrm{Si}}^2=1.66\times 10^{12}$. Thus, the quotient of Eq. (7) with each one of these parameters takes the values 0.006, 0.002, 0.0125, and 0.006, respectively. These small quotients ensure good approximations for the system crystal-vacuum; the contrast between the parameters of the crystal and the artificial vacuum is high, but yet numerically treatable allowing a good numerical convergence. It is worth saying that calculations for surface modes in 1D systems were made with these same criteria; our results are consistent with those already published but obtained with alternative semianalytical methods.[21] [In treating acoustic bulk waves, similar conditions for ρ and $c_{t,l}$ have been used by other authors when the vacuum is a crystal constituent. The condition involving the mass density and velocities has been written as the rate $\rho/c_{ijkl}\to 0$, where c_{ijkl} is the elastic constant tensor. In the isotropic approximation it is proportional to the square velocities. Thus the lower the mass density and more finite the sound velocities of the auxiliary medium, as in our system, the better the approximation for the vacuum properties.[11]]

III. NUMERICAL RESULTS

From a series of calculations for truncated crystals with complete cells at the surface, we concluded that surface modes exist, but only of mixed polarization. Calculations were made using a supercell with a crystal slab of nine complete cells. A basis of 841 plane waves was used to obtain the bulk solutions. For the case of surface waves, we employed 2025 waves; the solutions differ 0.25% and 0.55% from those obtained with 1865 and 1685 waves, respectively, which means acceptable convergence.

Figure 3 shows the band structure along the border of the Brillouin zone (the left side of the figure) and the projected bands on the [10] plane (the right side of the figure) for both shear ($u_x=u_y=0, u_z\neq 0$) and mixed ($u_x\neq 0, u_y\neq 0, u_z=0$) polarizations. On the right side we also include the dispersion curves of the surface modes. As can be seen, the structural and material selected parameters (see the figure caption) ensure the occurrence of a complete band gap not only in frequency but also in polarization that extends from 4.4 to

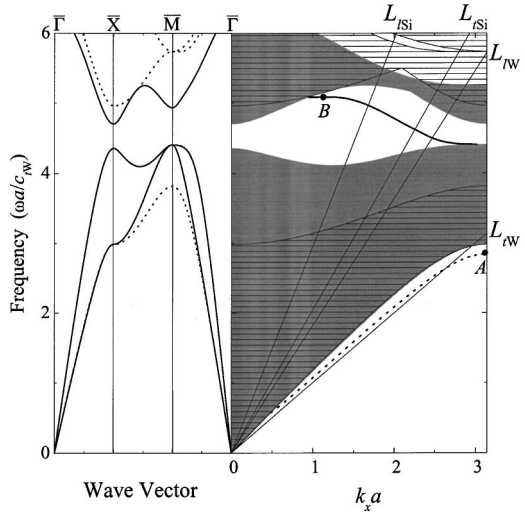

FIG. 3. Bulk band structure of a square array of W cylinders ($\rho = 19.3$ gr/cm^3, $c_l = 5.1\times10^5$ cm/s, and $c_t = 2.8\times10^5$ cm/s) in Si ($\rho = 2.42$ gr/cm^3, $c_l = 8.3\times10^5$ cm/s, and $c_t = 5.8\times10^5$ cm/s). The filling fraction is $f = 0.4$. The left panel shows the transverse (dashed curves) and mixed (continuum curves) modes along the border of the Brillouin zone. The projected bulk bands on the Γ-X direction and the dispersion curves of the surface modes are presented in the right panel. The lined regions correspond to transverse waves while the shaded regions are for mixed modes. The sound lines are lines of slope $L_{l,t} = \omega/c_{l,t}$.

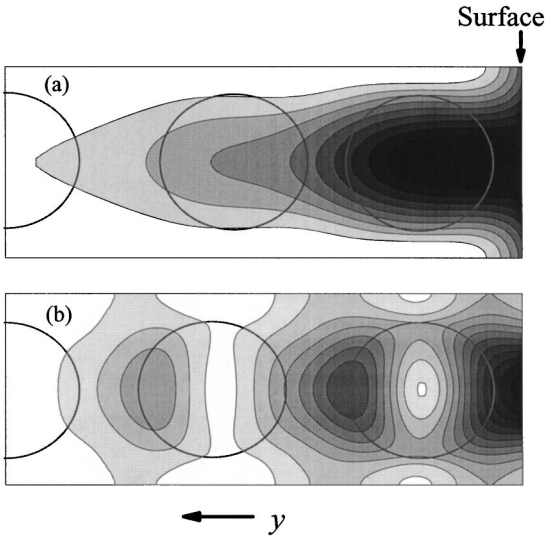

FIG. 4. Displacement intensity of the modes marked by dots in Fig. 3(a) The mode *A*, $(k_x d, \omega a/c_{tW}) = (\pi, 2.8)$, is of Rayleigh type because the intensity decays exponentially with some perturbation produced by the cylinders. (b) The mode *B*, (1.1, 5.1), corresponds to the surface modes with a damped oscillatory intensity. The displacement intensity of the two types of modes are confined to the last three crystalline layers.

4.7 in the reduced frequency units.

The specific characteristics of the surface modes in the dispersion curves depend on where they lay on the (k_x, ω) plane, to the right or to the left of each sound line [k_x higher or lower than $(\omega/c_{l,t})$ means an evanescent or oscillatory behavior of the corresponding longitudinal or transverse displacement inside the respective medium]. The surface modes near the zone boundary ($k_x a > 2.6$) in the lower curve of the dispersion are of Rayleigh type; they have a phase velocity lower than the velocities of the oscillatory solutions in W and Si resembling one of the Rayleigh mode characteristics. Figure 4(a) shows that the displacement intensity of these modes inside the crystal indeed decays as a Rayleigh mode, but is slightly perturbed by the crystal periodicity. For wave vectors lower than $k_x a = 2.6$ in the same curve the transverse displacement component has a small oscillation inside the W cylinders (the modes lie on the left vicinity of the W transverse sound line), making the modes slightly less localized at the surface.

Now, the surface modes in the second gap of Fig. 3 have different characters. Again, depending on where they are, the modes may even present a complete oscillatory behavior (with decay defined by an exponential envelope function). In such a case the localization of the elastic vibration at the surface results from scattering effects. The multiple Bragg reflections, a phenomenon also responsible for the occurrence of frequency gaps, confine the elastic vibration to the first three or four layers away from the surface. As an example Fig. 4(b) presents the displacement intensity of the mode *B* at $k_x a = 1.1$. The intensity, repetitive at each cell, already decays substantially in the third inner cell.

As an additional characteristic in Fig. 5 we plot the total intensity (shaded region) and the respective longitudinal (dotted curves) and transverse (dashed curves) contributions of the two types of surface modes discussed above. Let us remember that the longitudinal component at the surface is a compressional oscillation in the direction of the wave vector k_x (the surface wave propagates along the *x* direction). On the other hand, the transverse component is the shear contribution with a displacement in the *y* direction, the direction perpendicular to k_x. It is found that along the same dispersion curve the longitudinal and transverse contributions vary; apparently the polarization of the surface mode is mainly defined by the nearest sound lines. Figure 5 shows that mode *A* at the limit of the Brillouin zone in the lowest curve is practically transverse. However, mode *B* in the second gap is mainly longitudinal.

We may say that surface mode *B* in the second gap has much to do with the modes of the cells at the surface. Effectively, it is known that, inside the crystal, far from the surface, the vibrational modes of all the cells couple to form the bands. However, the modes of the last cells differ from those of the inner cells due to the lack of the half crystal (the last cells are stress free on one side). Thus, they do not couple to form bulk bands and separate from them appearing as surface modes. On the other hand, the Rayleigh type mode *A* appears because the composite has solid constituents with elastic properties. Because local pressure near the surface is lower than the pressure inside the crystal (there is a gradient of pressure), an appropriate perturbation will produce higher displacements near the surface than far from it. This mass displacement can support vibrational modes, the surface waves, that can be excited only by mixed waves—the compressional component is needed.

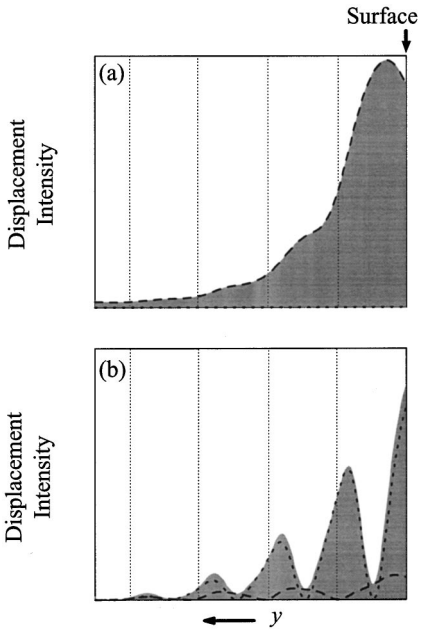

FIG. 5. Longitudinal and transverse contributions to the displacement intensities shown in Fig. 4. Dashed curves represent transversal (shear) vibrations and dotted curves correspond to longitudinal oscillations. The profiles are taken at the midcells along the y direction from the surface. The shaded regions are the total intensities. (a) The Rayleigh type surface mode *A* (b) The surface mode *B*.

We have not found shear surface modes when complete cells form the surface. This means that the vibrational shear modes of the last cells are not so different from the modes of the inner cells. Thus, all of them couple to form bands, with the modes of the last cells probably laying just at the band edges. What we have is preliminary numerical evidence that shear modes occur only when the termination leaves truncated cylinders at the surface. Of course this type of crystal truncation will modify the dispersion curves shown in Fig. 3 for mixed modes. However, an arbitrary truncation will be not discussed here; we have found that the additional structure at the surface makes the supercell method insufficient or inappropriate. Even employing many more waves for the displacement expansion (and much more machine memory) we were unable to find enough converged solutions. We concluded that in order to take into account the asymmetry of the last (truncated) cells, some other method for calculations is required.

We next explore the guidance of elastic wave in a Si layer grown at the surface of the truncated crystal (see Fig. 6). Wave guiding is expected because the crystal supports frequency gaps that will confine the elastic oscillations inside the layer. In some sense the guided modes in this *planar* waveguide can be considered as surface waves of the crystal-layer-vacuum system. We first evaluate the guided modes in a layer of thickness $d_l = a$, the same as the lattice constant. Because a is also the thickness of the crystal layers parallel to the additional homogeneous adlayer, we expect guided modes with frequencies on the order of the projected bands shown in Fig. 3.

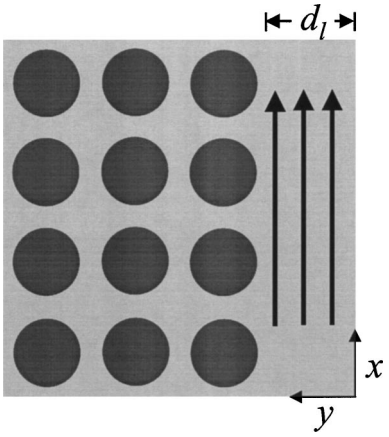

FIG. 6. Structure for wave guidance; a layer of thickness d_l is added at the top of the crystal. Although strictly we speak of guidance by the layer, we may see such solutions as surface modes of the complete system.

With this selection we found the modes whose dispersion curves are shown in Fig. 7. First we note that the curve shown by the dashed line for shear waves approaches the line $L_{t\mathrm{Si}}$ of the transverse bulk modes in homogeneous silicon. This is a known behavior for ordinary guidance: the dispersion curve of the guided waves converges asymptotically to the line of bulk propagation, with a perpendicular wave vector component of zero. Figure 7 shows that two mixed guided waves also appear in the second gap; as the frequency increases their dispersion curves penetrate into the second band, appearing again in the third gap. The most interesting

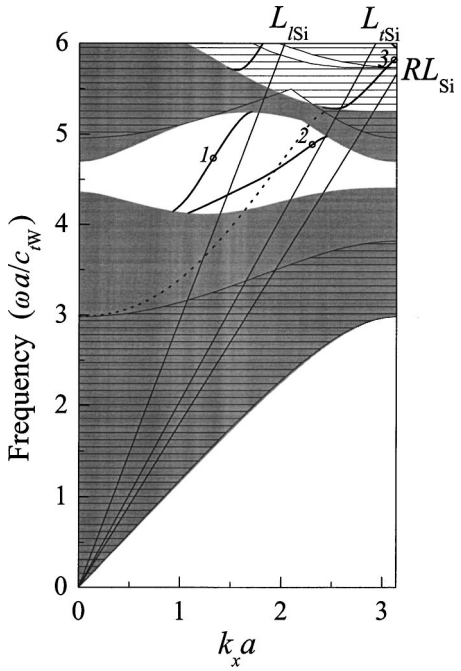

FIG. 7. Dispersion relations of transverse and mixed guided waves, dashed and continuum curves, respectively. The curves tend to one or the other sound line depending on their polarization. RL_{Si} is the Rayleigh line of Si (see the text). The curve at the right corner corresponds to modes that approach the Rayleigh behavior.

result is the tendency of the curve on the right. In the third gap it lies on the right side of the two sound lines, which means the modes do not have an oscillatory component inside the layer in the perpendicular direction away from the surface. However, the position of point 3 on the left side of the W sound lines allows oscillations in the cylinders to perturb the pure exponential decay in the Si. The dispersion curve tends to the line RL_{Si}, the Rayleigh line of silicon (the line of slope $\omega/k_x=5.05\times10^3$ m/s the phase velocity of the Rayleigh surface waves in Si).[22] The field profile for the modes marked in Fig. 7 are shown in Fig. 8. For the first two modes the nearness to the respective sound lines determines the main contribution, longitudinal or transverse, to the total intensity $|u|^2$. The third mode has a transverse component slightly more penetrating. In general the displacement profile of the modes along the same dispersion curve changes and the vibrational fields of modes with frequencies near the allowed bands penetrate more into the crystal.

As for ordinary guidance by a planar waveguide, we found that the number of guided waves for a given frequency depends on the adlayer thickness. Figure 9 shows the shear modes in the second gap when d_l varies from a to $5a$ at the fixed wave vector $k_xa=2$. More modes exist as the layer becomes thicker, and all their dispersion curves converge to the transverse sound line $L_{t\mathrm{Si}}$. We can make a rough estimation of the expected number of shear modes considering the Si layer as one of planar surfaces; the maximum number of modes can be written as

$$n_{\max}=\frac{d_l}{a\pi}\left(\frac{c_{t\mathrm{W}}^2}{c_{t\mathrm{Si}}^2}\Omega^2-(k_xa)^2\right)^{1/2},$$

where Ω is the reduced frequency. For example, at $\Omega=5.5$ and $k_xa=0.2$ it gives $n_{\max}=(d_l/a)0.55$. Thus with $d_l=2a$, $4a$, and $6a$ we have $n_{\max}\sim1$, 2, and 3, respectively. Figure 9 shows that this is a good estimation of the number of shear guided waves by the adlayer which will guide the elastic vibration only in frequency regions corresponding to PC band gaps.

On the other hand, a more rich behavior was found for the guided waves of mixed polarization. In Fig. 10 a series of panels show the modes in the second gap. With a very thin layer the solutions are of course the same as in Fig. 3. Figure 10(a) shows that surface modes of Rayleigh type disappear when $d_l=0.2a$; their dispersion curve merges with the lower band edge of the first band while the curve of surface modes in the second gap moves upward and the first guided modes appear just below the second band in the regime of low wave vectors. Panels (b), (c), and (d) present variations of the dispersion curves for thicknesses $d_l<a$. Panels (e) (f), and (g) for $d_l=2a$, $3a$, and $5a$, respectively, show that again more guided modes appear as the thickness of the layer increases. Now the two sound lines for silicon are relevant because in the regime of high frequencies the dispersion curves will converge to one of them. There exist, however, modes that lay beyond the two sound lines. As the guide becomes thicker they behave more and more like Rayleigh waves. Panel (f) shows that already for $d_l=3a$ their dispersion curve corresponds almost exactly to that of the Rayleigh surface waves of the single interface vacuum-silicon. This is an expected result because such modes have a finite decay distance. For a thick enough layer the presence of the periodic structure does not affect them. [For example, at the frequency $\omega a/c_{t\mathrm{W}}=4.5$ the Rayleigh wavelength of silicon in terms of the lattice constant is $\lambda_R=2.5a$ and the decay distance in the perpendicular direction to the surface of the transverse and longitudinal components are $\beta_t=0.8a$ and $\beta_l=0.5a$, respectively. Thus, for a thickness layer of order of λ_R or larger these guided modes are essentially ordinary Rayleigh modes.]

We finally remark that the surface modes of Rayleigh type shown in Fig. 3 have the complete characteristics of such a

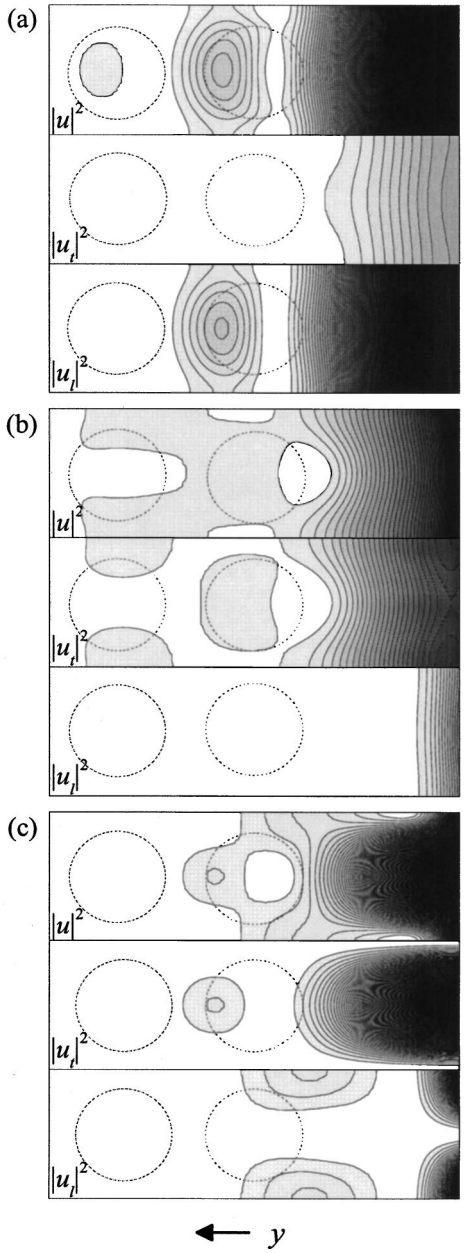

FIG. 8. The total displacement intensity and the transverse and longitudinal contributions of the three circled modes in Fig. 7. (a) Mode 1, $(k_xd,\omega a/c_{t\mathrm{W}})=(1.3,4.7)$. (b) Mode 2, (2.2, 4.8). (c) Mode 3, (π, 5.88).

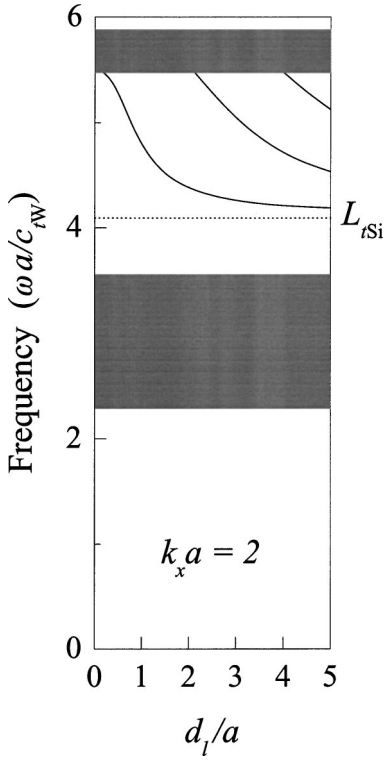

FIG. 9. Shear guided waves as function of d_l for the fixed wave vector $k_x a = 2$. One more mode arises when the thickness increases in $2a$, approximately.

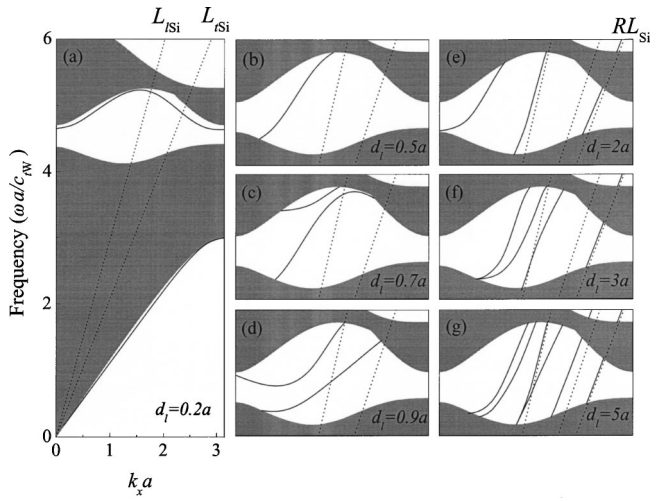

FIG. 10. Dispersion curves of mixed guided waves as function of d_l. Panel (a) shows that with a very thin layer the surface modes of Fig. 3 almost disappear giving place to the guided waves. Panels (b), (c), and (d) present the evolution of the curves prior the layer reaches $d_l = a$ (see Fig. 7). Panels (e), (f), and (g) show that one curve overlays the Rayleigh line while all the other converge to one or the other sound line.

mode, but do not correspond to one of the constitutive materials, as we have just discussed for the Si layer. They result from the periodicity of the medium and exist only below the first bulk band.

IV. CONCLUSIONS

We have found that surface elastic waves exist in truncated 2D phononic crystals of parallel W cylinders embedded in Si. The array is square and the plane of truncation was chosen parallel to a row of cylinders. With complete cells at the surface we found surface modes of mixed polarization only. Modes without counterparts in homogeneous systems arise due to scattering effects in the periodic structure—the Bragg reflections; these effects are also responsible for the elastic band gap occurrence. The elastic surface modes have an amplitude that vanishes in the perpendicular direction away from the surface, with profile either oscillatory (with an exponential envelope function) or exponential (like a Rayleigh wave). With the purpose of finding additional structural conditions for the localization of elastic vibrations at the surface, we have added a Si layer of thickness d_l above the truncated crystal. As d_l increases the surface modes disappear and the guidance of transverse and mixed vibrations by this *adlayer* begins. This special waveguide has the structure PC-Si-vacuum; therefore, in order to avoid a leakage of energy, the elastic guided waves may have frequencies corresponding to the PC band gaps only. For a thick enough adlayer we found that one of the solutions corresponds to the Rayleigh surface waves associated to the interface Si-vacuum; in such a case the PC is far enough from this interface to produce no appreciable perturbation.

ACKNOWLEDGMENTS

This work was supported by Consejo Nacional de Ciencia y Tecnología, CONACyT México. Grant No. 489100-5-35541-E. B.M.M. is grateful to CONACyT for support.

[1] M. Torres, F. R. Montero de Espinosa, D. García-Pablos, and N. García, Phys. Rev. Lett. **82**, 3054 (1999).
[2] D. Caballero, J. Sánchez-Dehesa, R. Martínez-Sala, C. Rubio, J. V. Sánchez-Pérez, L. Sanchis, and F. Meseguer, Phys. Rev. B **64**, 064303 (2001).
[3] D. García-Pablos, M. Sigalas, F. R. Montero de Espinosa, M. Torres, M. Kafesaki, and N. García, Phys. Rev. Lett. **84**, 4349 (2000).
[4] Ph. Lambin, A. Khelif, J. O. Vasseur, L. Dobrzynski, and B. Djafari-Rouhani, Phys. Rev. E **63**, 066605 (2001).
[5] You-Yu Chen and Zhen Ye, Phys. Rev. Lett. **87**, 184301 (2001).
[6] R. Sainidou, N. Stefanou, and A. Modinos, Phys. Rev. B **66**, 212301 (2002).
[7] M. S. Kushwaha, P. Halevi, L. Dobrzynski, and B. Djafari-Rohuani, Phys. Rev. Lett. **71**, 2022 (1993).
[8] C. Kee, J. Kim, H. Park, K. J. Chang, and H. Lim, J. Appl. Phys. **87**, 1593 (2000).
[9] J. O. Vasseur, P. A. Deymier, B. Chenni, B. Djafari-Rouhani, L.

Dobrzynski, and D. Prevost, Phys. Rev. Lett. **86**, 3012 (2001).
[10] L. Sanchis, A. Hakansson, F. Cervera, and J. Sánchez-Dehesa, Phys. Rev. B **67**, 035422 (2003).
[11] Y. Tanaka, Y. Tomoyasu, and S. Tamura, Phys. Rev. B **62**, 7387 (2000).
[12] J. O. Vasseur, P. A. Deymier, G. Frantziskonis, G. Hong, B. Djafari-Rouhani, and L. Dobrzynski, J. Phys.: Condens. Matter **10**, 6051 (1998).
[13] M. Kafesaki, M. M. Sigalas, and N. García, Phys. Rev. Lett. **85**, 4044 (2000).
[14] Y. Tanaka and S. Tamura, Phys. Rev. B **58**, 7958 (1998).
[15] J. O. Vasseur, P. A. Deymier, A. Khelif, Ph. Lambin, B. Djafari-Rouhani, A. Akjouj, L. Dobrzynski, N. Fettouhi, and J. Zemmouri, Phys. Rev. E **65**, 056608 (2002).
[16] C. Goffaux and J. Sánchez-Dehesa, Phys. Rev. B **67**, 144301 (2003).
[17] Y. Tanaka and S. Tamura, Phys. Rev. B **60**, 13 294 (1999).
[18] Elena V. Tartakovskaya, Phys. Rev. B **62**, 11 225 (2000).
[19] Y. Tanaka, and S. Tamura, Physica B **263–264**, 77 (1999).
[20] F. Ramos-Mendieta and P. Halevi, Phys. Rev. B **59**, 15 112 (1999).
[21] B. Manzanares-Martínez and F. Ramos-Mendieta, Phys. Rev. B **61**, 12 877 (2000).
[22] H. F. Pollard, *Sound Waves in Solids*, edited by H. J. Goldsmid, Applied Physics Series (Pion Limited, London, 1977).